Phonon Localization by Mass Disorder in Dense Hydrogen-Deuterium Binary Alloy

Phonon Localisation by Mass Disorder in Dense Hydrogen-Deuterium Binary Alloys

Ross T. Howie[1], Ioan B. Magdău[1], Graeme J. Ackland[1], Eugene Gregoryanz[1,*]
Alexander F. Goncharov[2]
[1] *School of Physics and Centre for Science at Extreme Conditions, University of Edinburgh, Edinburgh EH9 3JZ, UK.*
[2] *Geophysical Laboratory, Carnegie Institution of Washington, 5251 Broad Branch Rd. NW, Washington, DC 20015.*
(Dated: July 28, 2014)

Molecular hydrogen and deuterium crystals are made of the simplest atoms, yet when extreme conditions are applied, they exhibit a plethora of phenomena which represent many areas of condensed matter physics [1]. Solids can exist in para- and ortho- forms [2], have massive zero-point energy [2], adopt quantum and classical phases [1, 2] and are believed to display a pressure-induced insulating-to-semiconducting behaviour [3–6]. Effects such as atomic dissociation [7], superconductivity [8], re-entrant melting [9, 10] and superconducting/superfluid ground state(s) [11] are also predicted to occur. Here, using a combination of Raman spectroscopy and density functional theory calculations on dense hydrogen-deuterium mixtures, we find yet another text-book effect, mass-induced Anderson localisation of phonons [12–15]. We demonstrate that at 300 K and above 200 GPa dense hydrogen-deuterium mixtures transform into phase IV, forming a disordered binary alloy with 6 highly-localised intra-molecular vibrational (vibrons) and 4 de-localised low-frequency (<1200 cm^{-1}) modes. Hydrogen-deuterium mixtures are unique in showing a purely mass-induced localisation effect in the quantum solid: chemical bonding is isotope-independent while the mass varies by a factor of 2.

PACS numbers:

Recently, a new phase of hydrogen (and deuterium), phase IV, was discovered at 300 K and pressures above 230 GPa [4, 5]. Phase IV has two characteristic vibrons in the Raman spectra [4, 5]; by combining this observation with earlier density functional theory structure searches for phase III [16] it was proposed that this entropically-stabilised phase consists of two alternating graphene-like layers (*G*-layer) and "free-like" di-atomic molecules (*B*-layer) [5, 17–19] (see also Supplementary Information (SI)). The *B*-layer in hydrogen has a characteristic high vibron of ν_2 ∼4100 cm^{-1}, close to that in the gas state, a significant contributor to the zero-point energy (ZPE) compared with the much lower in energy ν_1 mode from the *G*-layer. Deuterium mass lowers the ZPE by a factor of $\sqrt{2}$ (ν_2 ∼3000 cm^{-1} for D_2), posing some interesting physical questions about the behaviour of dense hydrogen-deuterium mixtures in phase IV, since the two isotopes have quite different ZPE. It was theorised that that ZPE gain from the vibrational modes could favour segregation of D_2 molecules to the *B*-layer [16]. This segregation in 50:50 mixtures could lead to only 2 Raman-active vibrons with the *B*-layer mode having the characteristic frequency of D_2, while the *G*-layer mode will have the characteristic frequency of H_2. Such ZPE-driven ordering would be unique.

It is also possible that, in contrast to the ordering suggested by segregation, there could be atomic disorder with H_2:D_2 (and HD molecules spontaneously formed from the isotopes) distributed randomly across the lattice. In this case, the extreme isotopic mass ratio could raise another intriguing scenario: mass-induced Anderson localisation of phonons. Anderson localisation [13], is an unusual phenomenon where sufficient disorder on the lattice can break the very concept of electron or phonon band structures. Anderson localisation of phonons can be due to either disordered bond strengths or disordered masses, or both. In real systems it has previously been exceedingly difficult to disentangle these effects, since different elements have different chemical bonding and mass, while isotope mass effects are too small. Because of the identical chemical bonding and huge mass ratio in hydrogen-deuterium mixtures, the possibility of localisation exists, where the vibrational modes would be concentrated on a few molecules of similar type (*e.g.* H_2, D_2). Thus it appears that whether the mass difference drives ZPE ordering or localisation, interesting physics could be found in phase IV of hydrogen-deuterium mixtures.

In order to investigate these possibilities, we have used Raman spectroscopy combined with density functional theory (DFT) calculations on hydrogen-deuterium mixtures of varying concentrations (see SI, Refs. [5, 6, 20] and references therein for the experimental and calculation details). At 300 K, for pressures as low as 0.2 GPa, Raman spectroscopy in the fluid shows three vibrational modes (ν_1) (Fig. 1), demonstrating the formation of hydrogen deuteride (HD) molecules from an initial gas mixture of H_2+D_2 (see also Ref. [21]). The low-frequency (<1200 cm^{-1}) and vibrational modes of the mixtures correspond to a superposition of H_2, HD and D_2 spectra up to ∼195 GPa (Fig. 1). The low-frequency region at low pressures (< 20 GPa) shows a

superposition of rotational excitations corresponding to 3 molecular types, while with pressure increase, the modes broaden and eventually smear out forming a single relatively weak and broad peak around 410 cm^{-1} (Fig. 2a). In both experiment and calculations the Raman-active vibrons (ν_1-H_2, -HD or D_2) are higher than in pure materials but below those of the infrared vibrations, approaching the latter ones in the limit of small partial concentration. (see Fig. 2b and Refs. [22–24]). The ν_1-H_2, -HD and D_2 depend on the composition (Figs. 2b, 3 and Ref. [21]): the larger the molecular fraction - the closer the position of the vibrational band to that of a pure material, while the bands corresponding to smaller partial composition (impurity) have higher frequency. This observation can be partially understood based on the vibrational coupling model [2, 25], according to which the vibrational frequency is lowered due to the intermolecular coupling.

Above ∼195 GPa the Raman spectrum starts to change drastically and cannot be described as a superposition of H_2, D_2 and HD spectra. Between 195 and ∼210 GPa the broad peak at ∼410 cm^{-1} and vibrational (ν_1) modes split (Figs. 1 and 2), suggesting a phase transformation to phase IV. The splitting is similar to observed in pure H_2 or D_2 [5] although the splitting in mixtures appears to happen at slightly lower pressures. At pressures above 220 GPa, the low-frequency region forms 3 well-defined relatively narrow bands (marked $L_{1,2,3}$ in Figs. 1 and 2a) with L_1 ∼250 cm^{-1} becoming sharper and more intense with increasing pressure. At 270 GPa, the L_3 ∼1100 cm^{-1} mode splits off to form L_4 (Fig. 1, 2a) indicating the appearance of phase IV′, as documented for the pure H_2 [6]. If the H_2/D_2/HD isotopes were phase separated, 12 low-frequency and 6 vibrational modes would have been observed instead. If the H_2/D_2 were segregated, then only 2 vibrational modes would have been present, but there is no evidence for either. We note that with precisely four distinct modes, the low-frequency region for mixtures is equivalent to that of a single pure isotope in phase IV [5], indicating that all atomic species participate in these modes. The observed vibrational part of the spectrum can only be explained by contributions from H_2, D_2 and HD molecules in both G and B layers (Figs. 2b, 3). Following this scheme, the isolated B-layer peaks can be identified by simple mass scaling and by their slightly narrower appearance (Fig. 1). However, the assignment of the G-layer peaks is not straightforward since the observed lower-frequency vibrational modes form a complex density of state-like multifold (Figs. 1, 2 and 3) and their widths increase with pressure causing modes to overlap (Fig. 1). But more interestingly, the pressure dependence of the (ν_1) HD-G mode frequencies appears as a natural continuation of the (ν_2) DD-B mode, while (ν_1) HH-G appears as the continuation of (ν_2) HD-B vibration (Fig. 2b). The HH-G mode is extremely broad and surprisingly pressure independent, its mean value persisting at frequencies around 3450 cm^{-1}. The HH-G band also appears to be relatively weaker and broader (due to re-distribution to its intensity) than the ones from D_2 and HD.

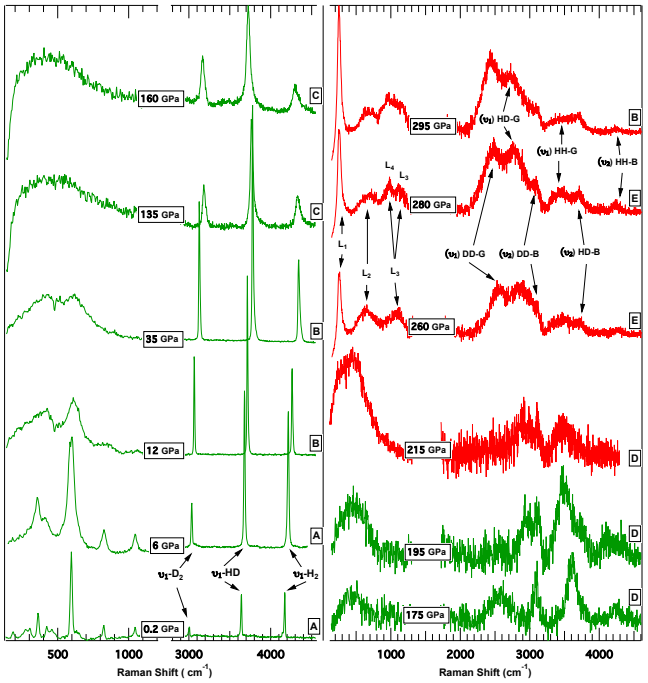

FIG. 1: Representative Experimental Raman spectra of H_2-D_2 mixtures. The spectra from different runs at room temperature are labeled by the capital letters A, B, C, D and E and marked with the nominal pressures at which spectra were collected. The strong first order diamond Raman at above 1333 cm^{-1} was removed for clarity. The spectra obtained with 514 nm laser excitation line are shown in green while the spectra obtained with 647 nm are shown in red. The ratio of the isotopes in run A is 60:40 (H:D); 55:45 in B and C and 50:50 in D and E. The different sizes of the sample chambers in the presented runs, different H:D ratios and the varying Raman efficiency and spectral throughput of different detectors make the comparison of the intensities unreliable. Note that the vibrational parts of the spectra between 215 and 295 GPa have their intensities re-normalised to correct for the decreasing sensitivity of the detector at higher energies.

We have analysed the disordered system using *ab initio* lattice dynamics (LD) (at T=0 K) and molecular dynamics (MD) (T=300 K) simulations of phase IV, based on the P_c structure proposed in Ref. [17]. Free energy calculations from LD (Fig. S1) show that the ZPE gain in the vibron modes is offset by frequency shifts elsewhere, and the free energy of ordering is too small to drive isotopic segregation in phase IV. Thus theory and experiment agree that segregation of the layer due to the ZPE-driven ordering does not occur. Our LD calculations demonstrate that the mass disorder gives vibrational eigenmodes very different from the pure isotopes, exhibiting a strong localisation tendency. In this regime, the vibrations in the G-layer involve all molecu-

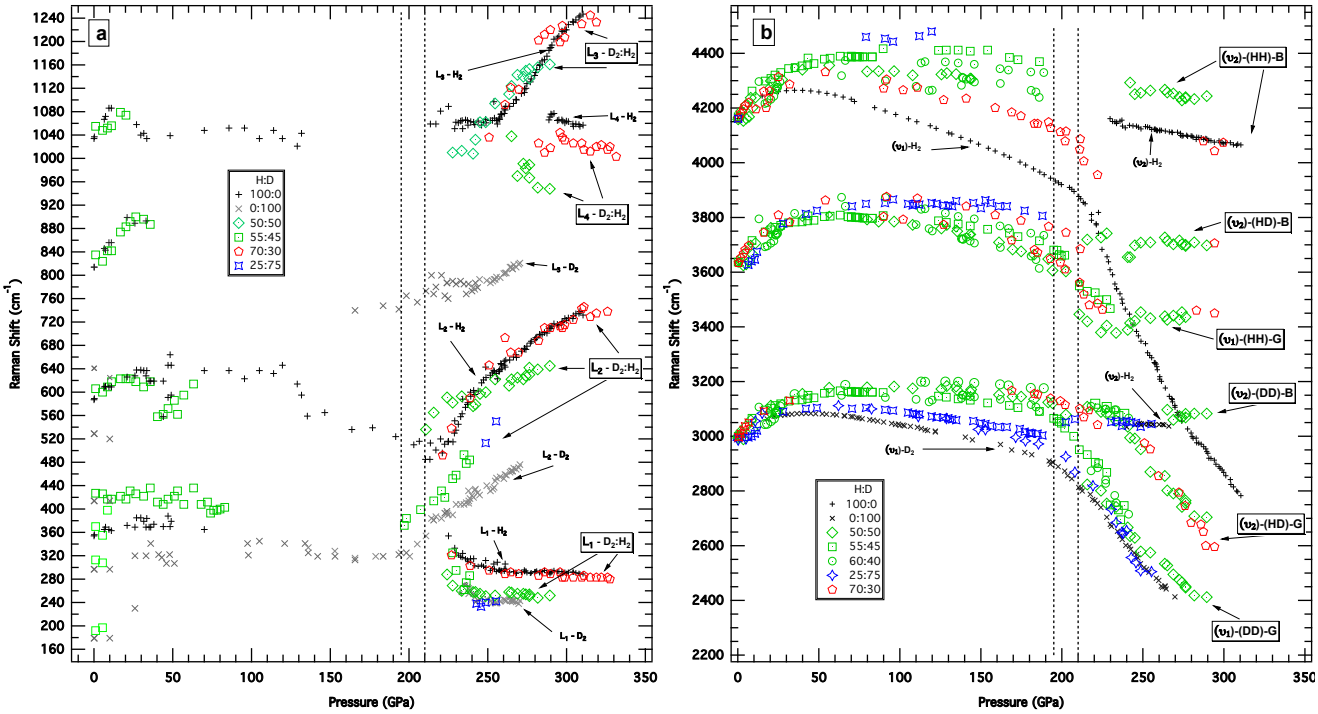

FIG. 2: Experimental pressure dependencies of the Raman low-frequency (A) and vibrational (B) bands observed in H_2-D_2 mixtures.The coloured symbols represent the frequencies from the mixtures and small grey "x" and black "+" are the frequencies of pure D_2 and H_2 from Ref. [5, 6]. The same colour represents the same ratio of H:D with the exact numbers given in the legend. The vertical black dashed lines at 195 and 210 GPa indicate the pressure range at which librational and vibronic modes undergo significant changes and split.

lar types, (Fig. 3). The precise amount of localisation varies depending on the isotope composition (see Figs. 4, S2), The localisation varies asymmetrically with concentration, reaching maximum at around 40% H. The H-H modes at low H concentrations are more localised than equivalent D-D modes at low D concentrations and with rising pressure, the localisation is increasingly shifted towards D rich mixtures (Fig. S2). For each molecular species, the maximal localisation per mode occurs when the concentration of that species in the mixture is small (Figs. 4 and S2). However, closer to 50% H, the number of localised modes is larger, thus maximising the total localisation (Fig. 4). Figures 4 and S2 demonstrate localisation, more pronounced for lighter molecular species. This is in excellent agreement with our Raman spectra which show broad coupled vibrational modes skewed towards heavier isotopes of the G-layers and narrow uncoupled B-bands (Fig. 1).

We also carried out a detailed theoretical analysis of vibrational eigenvectors to determine the Raman activity of modes. This also shows that localisation causes many more modes to acquire Raman activity than is the case for H_2 and D_2. In Fig. 3 we compare these predictions with experimental results at similar conditions. With lattice dynamics (LD) averaged over many mixture configurations, we find excellent agreement with experiments for the peak widths, and the variation in Raman shifts with concentration and pressure. The Raman frequencies for the B-vibrations are also in good agreement.

Two well separated, nearly pressure-independent, bands near 4300 and 3700 cm^{-1}, come from HH-B and HD-B vibrations respectively. The HH-B vibrational modes frequencies are predicted and observed to decrease with increased H concentration as the modes become less localised, while the HD-B modes have a minimum frequency at 50% (Fig. 3). By inspecting the eigenvectors (Fig. S3), we can relate localisation to the number of neighbouring H_2 molecules. An isolated H_2 molecule will typically have a localised mode associated with itself. Groups of adjacent molecules have modes localised across the group, which can be associated with intermolecular coupling which, typically, lowers the frequency of the in-phase (Raman active) vibron. concentration, larger coupled H_2 groups are present, reducing the Raman frequency still further. For similar reasons, the DD-B and DD-G Raman frequencies soften with increased D concentration, and the HD-B Raman mode is softest around 50:50 mixtures, when HD molecules are most abundant.

The remaining modes are localised on molecules of different types. The DD-B vibration couples to the HH-G vibration in LD calculation. However, in MD the G-

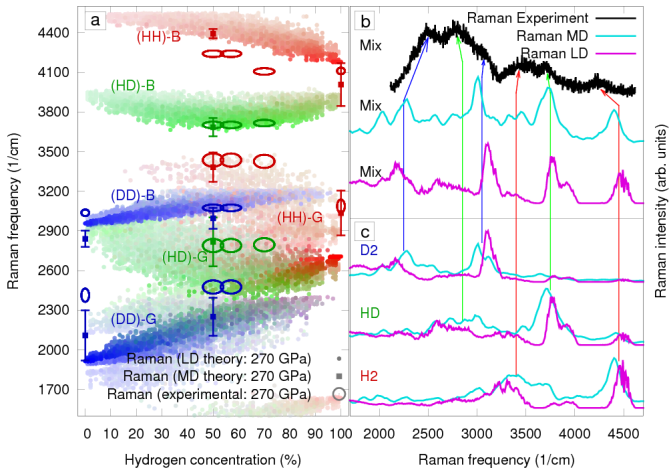

FIG. 3: Comparison of calculated and measured Raman spectra at 270 GPa. Panel a: The most intense Raman modes for 2700 different LD calculations (one coloured solid dot per mode) at 270 GPa and various concentrations. The colour is assigned by calculating RGB ratios based on the partial Raman contributions from each molecular species: H_2 (red), HD (green) and D_2 (blue) with the saturation proportional to the Raman intensity. The Raman experimental data is plotted with ellipses where the axes represent the errors in concentration and frequency. Colours demonstrating the character of each mode were attributed by observing the behaviour of the spectra with pressure in the experiments. MD (coloured solid rectangles) show peaks of the Fourier-transformed autocorrelation projection function. Differences from the LD come from including dynamical effects such as the librations of trimer motifs (see also SM). Panel b: Detailed theory-experiment comparison of the Raman spectra at 270 GPa and 50:50% H_2-D_2 mixtures. Experimental resolution error is not included in the MD and LD results. Panel c: Individual contributions of different molecular species calculated with both LD and MD. The correspondence between individual modes is illustrated with arrows. Theory agrees well with experiment once MD calculations are used to improve LD frequencies.

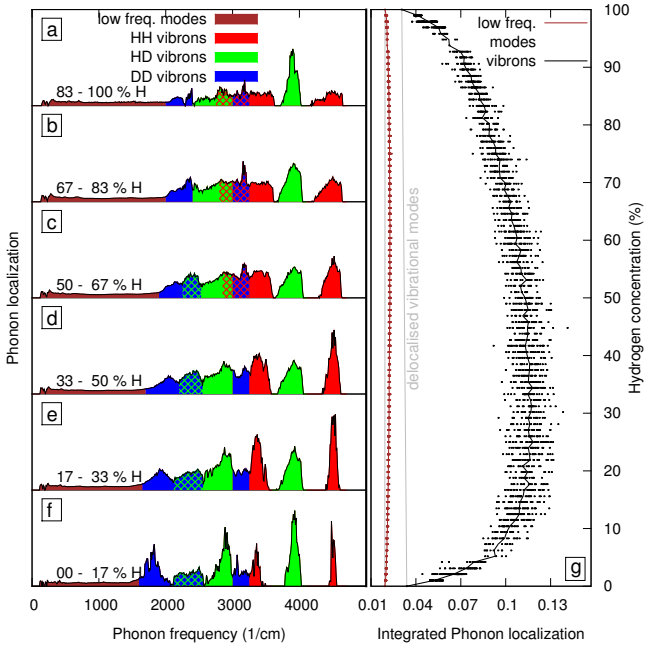

FIG. 4: Calculated phonon localisation at 270 GPa.Panels a-f: Calculated localisation inverse participation ratio per mode as a function of frequency for different H concentration ranges. Shaded brown are the low-frequency modes, that show no localisation. Red, green and blue shades indicate vibrons involving mainly H_2, HD and D_2 respectively, with considerable overlap for D_2-B and G modes. Panel g: Localisation as a function of concentration for vibrational (black) and low-frequency modes (brown). IPR from the delocalised limit of pure H_2 and D_2, are illustrated in light grey. The skewed maximum shows that that isolated H_2 molecules in the B-layer produce strongly localised vibrations, whereas isolated B-layer D_2 molecules couple to HD and H_2 molecules in the G-layers (H_2 molecules are more likely to be isolated if their concentration is low).

layer vibrations have higher frequencies, and thus DD-B is coupled more strongly to HD-G modes (Fig. 3). This explains why HD-G overlaps with the DD-B mode in the experiment (Fig. 2b). By contrast, the G modes are more delocalised and strongly hybridised. Above 50% H concentration, DD-B, HH-G and HD-G have very similar frequencies and generate a broad, complex Raman-signal as seen experimentally. Eigenmodes can no longer be assigned to a single molecular species, in particular, HH-G mode couples heavily to the HD-G vibrations. Due to this strong coupling, HH-G does not show the characteristic softening with increasing pressure (Figs. 2b, and S4, S5).

As shown previously [19], the Raman frequency of the G-vibrations is sensitive to temperature. We used MD projection to investigate for this (see SI), and we see that temperature increases the frequency-shifts into better agreement with experiment. The MD shows localisation, but does not permit the necessary level of configurational sampling for quantitative analysis of concentration and distribution.

We do not see any mode localisation for the low-frequency ($L_{1,2,3,4}$) excitations (Figs. 2a and 4). These modes either involve motion of large units such as G-layer trimers or inter layer modes. The L_1 mode (trimer-libration) characteristic of phase IV in pure $H_2(D_2)$ is observed following either the pure H_2 frequencies in the H rich mixtures or D_2 frequencies in 50:50 and D rich samples (Fig. 2a). This observation is in agreement with highly anharmonic nature of these modes [6, 19, 26].

The reproduction of frequencies and widths is evidence that simulation and experiment are looking at the same phase IV structure. The key observable signature of localisation lies in the concentration dependence (Figs. 2 and 3). For each species (H_2, HD and D_2) more-localised modes have higher Raman frequency, thus the H2 data (Fig 3a) has negative slope, the D2 data positive and the

HD peaked about 50% concentration.

Anderson localisation has been demonstrated in several systems including light [27], sound [28] and Bose-Einstein condensates [29]. This study has turned the spotlight onto the equivalent phonon phenomenon, driven purely by mass disorder. Hydrogen isotopes are the only physical candidate for Anderson localisation of phonons due only to isotope mass. Indeed, for simple lattices, even a 2:1 mass-ratio is insufficient to cause localisation [15], however the inhomogeneity between inter- and intramolecular bonds circumvents this theoretical limit allowing localisation of vibrons in $H_2/HD/D_2$ mixtures. Phase IV of hydrogen(s) is an unique system where there is a crossover between intramolecular, intermolecular and quantum energy scales with the ratio of phonon energies almost 20:1, providing the route for the localisation despite the small mass ratio.

This work was supported by a research grant from the U.K. Engineering and Physical Sciences Research Council.

[1] J.M. McMahon, M. Morales, C. Pierleoni, D.M. Ceperley, Rev. Mod. Phys. **84**, 1607 (2012).
[2] J. van Kranendonk, J. Solid hydrogen. theory of the properties of solid h2, hd and d2 (1983).
[3] P. Loubeyre, F. Occelli, R. LeToullec, Nature **416**, 6881 (2002).
[4] M.I. Eremets, I.A. Troyan, Nat. Mat. **10**, 927, (2011).
[5] R.T. Howie, C.L. Guillaume, T. Scheler, A.F. Goncharov, E. Gregoryanz, Phys. Rev. Lett. **108**, 125501 (2012).
[6] R.T. Howie, T. Scheler, C.L. Guillaume, E. Gregoryanz, Phys. Rev. B. **86**, 214104 (2012).
[7] E. Wigner, H.B. Hungtington, J. Chem. Phys. **3**, 764 (1935).
[8] N.W. Ashcroft, Phys. Rev. Lett. **21**, 1748 (1968).
[9] E. Gregoryanz, A.F. Goncharov, K. Matsuishi, H.K. Mao, R.J. Hemley, Phys. Rev. Lett. **90**, 175701 (2003).
[10] S. Bonev, E. Schwegler, T. Ogitsu, G. Galli, Nature **431**, 669 (2004).
[11] E. Babaev, A. Sudbø, N.W. Ashcroft, Nature **431**, 666 (2004)
[12] F.J. Dyson, Phys. Rev. **92**, 6 (1953).
[13] P.W. Anderson, Phys. Rev. **109**, 1492 (1958).
[14] A. Lagendijk, B. van Tiggelen, D. Wiersma, Physics Today **62**, 24 (2009).
[15] C. Monthus, T. Garel, Phys. Rev. B. **81**, 22 (2010).
[16] C.J. Pickard, R.J. Needs, Nat. Phys. **3**, 473 (2007).
[17] C.J. Pickard, M. Martinez-Canales, R.J. Needs, Phys. Rev. B. **85**, 214114 (2012).
[18] H. Liu, L. Zhu, W. Cui, Y. Ma, J. Chem. Phys **137** 074501 (2012).
[19] I.B. Magdau, G.J. Ackland, Phys. Rev. B. **87**, 174110 (2013).
[20] R.T. Howie, E. Gregroyanz, A.F. Goncharov, J. Appl. Physics **114**, 073505 (2013).
[21] D.M. Brown, W.B. Daniels, Phys. Rev. A. **45**, 6429 (1992).
[22] P. Loubeyre, P. Occelli, P. Dumas, Phys. Rev. B. **87**, 134101 (2013).
[23] M.I. Eremets, I.A Troyan, Ph. Lerch, A. Drozdov, High Pres Res. **33**, 377 (2013).
[24] C.S. Zha, Z. Liu, M. Ahart, R. Boehler, R.J. Hemley, Phys. Rev. Lett. **110**, 217402 (2013).
[25] P. Loubeyre, R. LeToullec, J.P. Pinceaux, Phys. Rev. B. **45**, 12844 (1992).
[26] A.F. Goncharov, J.S. Tse, H. Wang, J. Yang, V.V. Struzhkin, R.T. Howie, E. Gregroyanz, Phys. Rev. B. **87**, 024101, (2013).
[27] M. Segev, Y. Silberberg, D.N. Christodoulides, Nat. Photon. **7**, 197, (2013).
[28] H. Hu, A. Strybulevych, J.H. Page, S.E. Skipetrov, B.A. van Tiggelen, Nat. Phys. **4**, 945 (2008).
[29] G. Roati, C. D'Errico, M. Fattori, C. Fort, M. Zaccanti, G. Modugno, M. Modugno, M. Inguscio, Nature **453**, 895 (2008).
[30] Y. Akahama, H. Kawamura, Jouranl of Physics: Conference Series **215**, 012195 (2010).
[31] M. Marques, M. Santoro, C.L. Guillaume, F.A. Gorelli, J. Contreras-Garcia, R.T. Howie, A.F. Goncharov, E. Gregoryanz, Phys. Rev. B. **83**, 184106 (2011).
[32] F.A. Gorelli, S.F. Elatresh, C.L. Guillaume, M. Marques, G.J. Ackland, M. Santoro, S.A. Bonev, E. Gregoryanz, Phys. Rev. Lett. **108**, 055501 (2012).
[33] G.J. Ackland, I.B. Magdau, High Pres. Res. **34**, 198 (2013).
[34] F. Evers, A.D. Mirlin, Rev. Mod. Phys. **80**, 1355 , (2008).